(2)

AD-A243 094

REPORT DOCUMENTATION PAGE

	1b RESTRICTIVE MARKINGS
2b DECLASSIFICATION / DOWNGRADING SCHEDULE	3 DISTRIBUTION / AVAILABILITY OF REPORT unlimited
4 PERFORMING ORGANIZATION REPORT NUMBER(S) 8	5 MONITORING ORGANIZATION REPORT NUMBER(S) ONR
6a NAME OF PERFORMING ORGANIZATION NIST	6b OFFICE SYMBOL (If applicable)
7a NAME OF MONITORING ORGANIZATION ONR	
6c ADDRESS (City, State, and ZIP Code) A329, Materials Building Gaithersburg, MD 20899-0001	7b ADDRESS (City, State, and ZIP Code) Code 1131 800 N. Quincy Street Arlington, VA 22217-5000
8a NAME OF FUNDING / SPONSORING ORGANIZATION ONR	8b OFFICE SYMBOL (If applicable)
9. PROCUREMENT INSTRUMENT IDENTIFICATION NUMBER N0014-90-F-0011	
8c ADDRESS (City, State, and ZIP Code)	10 SOURCE OF FUNDING NUMBERS

PROGRAM ELEMENT NO	PROJECT NO	TASK NO	WORK UNIT NO

11 TITLE (Include Security Classification)
Determination of the Optical Constants of Thin Chemical-Vapor-Deposited Diamond Windows From 0.5 To 6.5 eV

12 PERSONAL AUTHOR(S)
Lawrence H. Robins, Edward N. Farabaugh and Albert Feldman

13a TYPE OF REPORT	13b TIME COVERED	14 DATE OF REPORT (Year, Month, Day)	15 PAGE COUNT
interim	FROM _____ TO _____	91-9-27	13

16 SUPPLEMENTARY NOTATION

17 COSATI CODES		
FIELD	GROUP	SUB-GROUP

18. SUBJECT TERMS (Continue on reverse if necessary and identify by block number)
This document has been approved for public release and sale: its distribution is unlimited.

19 ABSTRACT (Continue on reverse if necessary and identify by block number)

The optical constants of thin chemical-vapor-deposited diamond windows were determined as a function of photon energy from 0.5 to 6.5 eV by fitting experimental transmittance and reflectance data to a model that includes the effects of surface optical scatter. Root-mean-squared surface roughness values were also obtained from the analysis. The windows were fabricated by microwave-plasma-assisted CVD on silicon substrates, followed by partial removal of the substrates by etching. The values of the refractive index were found to be comparable to or slightly less than the values for single-crystal gem diamonds. Substantial absorption was found to occur in the visible to near-ultraviolet region (2 to 5 eV) where single-crystal diamond is transparent. The spectrum of the low-energy absorption is well-described by the Taucs function, which is used to fit the absorption spectrum of "diamondlike" amorphous carbon. There is a steep increase in absorption above the indirect bandgap of diamond (5.5 eV). The magnitude of the high-energy absorption edge is larger than in single-crystal diamond, and the shape is approximately exponential.

20 DISTRIBUTION / AVAILABILITY OF ABSTRACT	21 ABSTRACT SECURITY CLASSIFICATION
☒ UNCLASSIFIED/UNLIMITED ☐ SAME AS RPT ☐ DTIC USERS	unclassified

22a NAME OF RESPONSIBLE INDIVIDUAL	22b TELEPHONE (Include Area Code)	22c OFFICE SYMBOL

DD FORM 1473, 84 MAR — 83 APR edition may be used until exhausted. All other editions are obsolete. SECURITY CLASSIFICATION OF THIS PAGE

Enclosure (3)

OFFICE OF NAVAL RESEARCH

Contract N00014-90-F-0011

R&T Project No. IRMT 025

TECHNICAL REPORT No. 8

DETERMINATION OF THE OPTICAL CONSTANTS OF THIN CHEMICAL-VAPOR-DEPOSITED DIAMOND WINDOWS FROM 0.5 TO 6.5 eV

Lawrence H. Robins, Edward N. Farabaugh and Albert Feldman

submitted to

SPIE PROCEEDINGS 1534, DIAMOND OPTICS IV

National Institute of Standards and Technology

Ceramics Division

Gaithersburg, MD 20899

September 27, 1991

Determination of the optical constants of thin chemical-vapor-deposited diamond windows from 0.5 to 6.5 eV

L. H. Robins, E. N. Farabaugh and A. Feldman

National Institute of Standards and Technology
Ceramics Division
Gaithersburg, MD 20899

ABSTRACT

Transmittance and reflectance spectra of chemical-vapor-deposited (CVD) diamond windows with thicknesses from 0.4 to 1.9 μm were measured in the 0.5-6.5 eV photon energy range. The windows were fabricated by microwave-plasma-assisted CVD on silicon substrates, followed by partial removal of the substrates by etching. Three spectra were measured for each window, the reflectance of the top surface, the reflectance of the bottom surface (the surface exposed by etching), and the transmittance. The optical constants were determined as a function of photon energy by fitting the data to a model that includes the effects of surface optical scatter. Root-mean-squared (r.m.s.) surface roughness values were also obtained from the analysis. The values of the refractive index (n) were found to be comparable to or slightly less than the values for single-crystal gem diamonds. The values of n were lowest in the most defective films. The absorption coefficient (α) differs from that of single-crystal diamond. In some films, substantial absorption occurs in the visible to near-ultraviolet region (2 to 5 eV) where single-crystal diamond is transparent. The spectrum of this low-energy absorption is well-described by the Taucs function, which is used to fit the absorption spectra of "diamondlike" amorphous carbon materials. There is a steep increase in α at photon energies at and above the indirect bandgap of diamond (5.5 eV). The absorption rises more steeply from 5.5 to 6.5 eV in these films than in single-crystal diamond, and the shape of the high-energy absorption edge is approximately exponential.

1. INTRODUCTION

Diamond has an exceptionally wide intrinsic transparency range, from 0.23 μm in the ultraviolet (UV) to 2.5 μm in the mid-infrared (IR), and also from 6.5 μm to >100 μm in the far-IR region. Because of its excellent transparency and other superior properties (e.g., high hardness), there is great interest in utilizing synthetic diamond as a bulk optical material or as a thin-film optical coating material.[1] At present, much of the applications interest is focussed on the mid-to-far-IR, but transmissive optical components for the UV, visible, or near-IR regions are also possible.

Chemical-vapor-deposited (CVD) diamond films have a polycrystalline growth habit when grown on nondiamond substrates. The faceted surfaces of the polycrystalline films give rise to optical scatter, which reduces both the transmittance and the reflectance.[2] The size and shape of the facets can be controlled to some extent by control of the nucleation and growth conditions, but even the finest-grained polycrystalline films suffer large scatter losses in the visible-UV region.[3] Extrinsic absorption, due to defects, impurities, or non-diamond phases, may also degrade the transmittance. In order to improve the performance of CVD diamond as a transparent material, it is important to know whether transmittance losses are due

to absorption or to surface scatter. Surface scatter can be reduced by post-deposition polishing treatments,[4,5] but extrinsic absorption can, in most cases, be reduced only by modifying the deposition conditions. (Some of the absorbing defects might be destroyed by thermal annealing after deposition, although we do not know of any observation of this effect in CVD diamond).

The refractive index is also an important parameter for optical applications. If, for example, CVD diamond is used as an anti-reflection coating on a higher index substrate, then the magnitude of the anti-reflection effect will be determined by the relationship between the refractive indices of the film and substrate. It is thus desirable to have optical constant data for CVD diamond films, including both the refractive index (n) and the absorption coefficient (α). The absorption coefficient (α) is related to the dimensionless attenuation constant (k) by the equation $\alpha = 4\pi k/\lambda$, where λ is the vacuum wavelength.

We undertook the present study with the goal of determining the optical constants of thin, fine-grained polycrystalline diamond films from 0.5 to 6.5 eV, or 0.19 to 2.5 μm. We will show here that by measuring the specular reflectance (from both surfaces) and transmittance spectra of unsupported diamond windows, one can obtain sufficient information to determine the optical constants in the presence of large surface scatter losses. In particular, bulk absorption can be distinguished from surface scatter when both effects are of the same order of magnitude.

2. EXPERIMENTAL PROCEDURE

The diamond films were grown on 2.54 cm diameter (100) oriented silicon wafers in a commercial microwave-plasma-assisted CVD reactor. To increase the nucleation density of diamond particles, the substrates were prepared by abrasive hand-polishing with 1 μm size diamond powder.[6] The deposition conditions were: gas mixture, 0.2% to 2.0% CH_4, remainder H_2; nominal substrate holder temperature, 800° C; microwave power, 600 W; pressure, 1.4×10^3 Pa; total gas flow rate, 260 cm^3/min. These relatively low-power and low-pressure conditions were selected because they produce films of more uniform thickness than higher power/pressure conditions, as noted in a previous study.[3] (Because of substrate heating by the plasma, and poor thermal contact between the substrate and holder, the actual temperature at the substrate surface was probably higher than 800° C.)

Four films were grown, with the following deposition conditions: film #1, 0.2% CH_4, deposition time, 7 hours; film #2, 0.5% CH_4, 2.7 hours; film #3, 2.0% CH_4, 1.7 hours; film #4, 2.0% CH_4, 7 hours. After deposition, an unsupported diamond window was formed in each specimen by etching a 1.2 cm diameter circular hole in the silicon substrate.

Specular transmittance and reflectance spectra were recorded in a UV-visible-IR dual-beam spectrophotometer. For each film, reflectance spectra were measured both with light incident on the top surface and with light incident on the bottom surface (the surface exposed by etching). For film #2, transmittance spectra were measured both with light incident on the top surface and with light incident on the bottom surface; comparison of these spectra verified that the transmittance is not changed by reversal of the propagation direction. The angle of incidence was normal to the film surface for the transmittance measurements, and 11° to the normal for the reflectance measurements. A 0.8 cm diameter aperture was used to ensure that, for a given specimen, the illuminated region of the window did not vary from one

measurement to another. Each spectrum was recorded in two overlapping ranges; a tungsten lamp and PbS photocell were used for the first range, 500-2500 nm (0.5-2.5 eV); a deuterium lamp and photomultiplier tube were used for the second range, 190-600 nm (2.1-6.5 eV). Reflectance spectra were normalized by comparison to a standard mirror (Al/MgF_2) whose reflectance is known to within 2%.

Details of the experimental apparatus for Raman spectroscopy[7] have been presented elsewhere. Raman scattering was excited by the 514.53 nm line of an Ar^+ laser with incident power of ~100 mW. The wavenumber scale for the Raman spectrum was calibrated to an accuracy of ~0.1 cm^{-1} by the use of the atomic spectral lines of argon and neon vapor lamps.

3. EXPERIMENTAL RESULTS

3.1. Transmittance and reflectance spectroscopy

The transmittance and reflectance spectra of films #1 to #4 are plotted in Fig. 1(a)-1(d), respectively. Each figure contains three spectra, the transmittance and the reflectances from the top and bottom surfaces of the window. For conciseness, we will call the transmittance T, the film reflectance for light incident on the top surface R_1, and the film reflectance for light incident on the bottom surface R_2. Some general qualitative features of these spectra are pointed out here; a quantitative analysis is provided in the following section. All of the spectra show interference fringes, which arise from phase-coherent multiple reflections from the top and bottom surfaces. The interference fringe spacing is inversely proportional to the product of the film thickness and refractive index. Thus, the fringes are most closely spaced for film #4, which is several times thicker than the other films. Also, the fringe spacing for a given film decreases with increasing photon energy, which is especially observable in the UV region, because the refractive index increases with increasing photon energy.

For all spectra, both the interference fringe amplitude and the average intensity (midway between the interference maxima and minima) decrease with increasing photon energy. When the T, R_1, and R_2 spectra for a given film are compared, the following trends can be seen. The interference amplitude decreases most rapidly with increasing photon energy for T, next most rapidly for R_2, and least rapidly for R_1. On the other hand, the average intensity decreases least rapidly for R_2. R_2 is significantly larger than either R_1 or T at the maximum photon energy. We will show that these effects are due to a combination of surface scatter and bulk absorption.

3.2. Raman spectroscopy

Raman spectra[7] of films #1 to #4 are shown in Fig. 2. All spectra are plotted together for comparison in Fig. 2(a); the spectra of films #3 and #4 are replotted on an expanded scale in Fig. 2(b) to better display their fine structure. Note that the spectra have been multiplied by scale factors for ease of visual comparison; the scale factors were selected to make the apparent intensity of one feature (the broad peak at ~1500 cm^{-1}) the same in each spectrum. Also, the spectra are offset vertically to avoid overlap. Finally, the photoluminescence (or, equivalently, fluorescence) background, which is commonly observed in the Raman spectroscopy of CVD diamond, was subtracted from each spectrum by numerical fitting to a polynomial function. The photoluminescence background before subtraction was several times more intense for films #1 and #2 than for films #3 and #4. Statistical

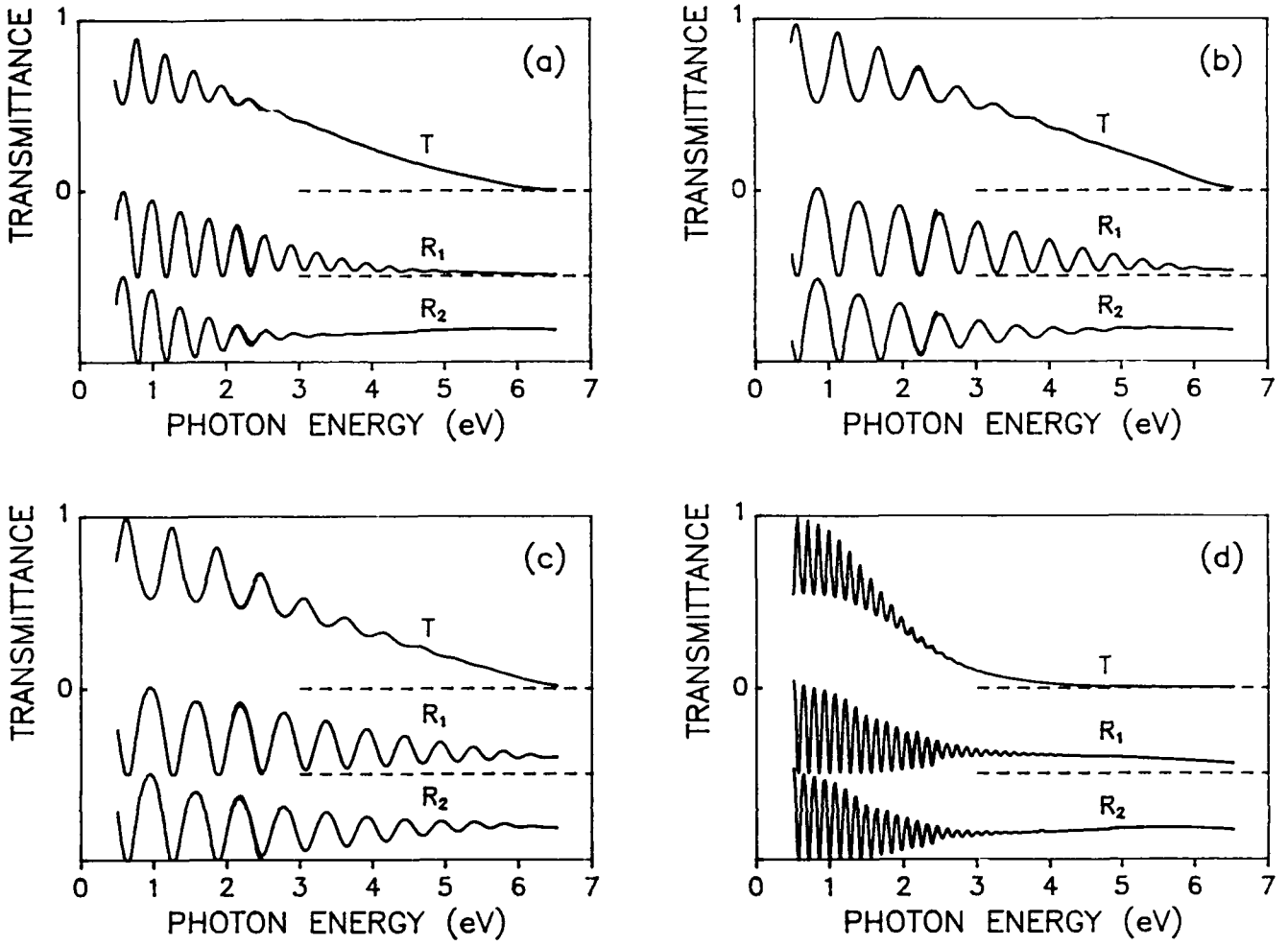

Fig. 1. Transmittance (T), top reflectance (R_1) and bottom reflectance (R_2) of four diamond films. T, R_1, and R_2 spectra are offset vertically but drawn to the same scale; the full length of the vertical axis is 200% of full scale. (a) Film #1: grown from 0.2% CH_4 in H_2 mixture, 0.66 μm thick. (b) Film #2: 0.5% CH_4, 0.46 μm thick. (c) Film #3: 2.0% CH_4, 0.42 μm thick. (d) Film #4: 2.0% CH_4, 1.9 μm thick.

fluctuations in the photoluminescence background give rise to noise which cannot be eliminated by subtraction; this explains the relatively high noise level in the spectra of films #1 and #2.

The Raman signature of crystalline diamond is a narrow line at 1332 cm^{-1}. A narrow line at approximately this wavenumber can be seen in each spectrum, but the relative intensity of the narrow line, compared to the other spectral features, decreases with increasing methane fraction in the deposition process (0.2% for #1, 0.5% for #2, and 2.0% for #3 and #4). The peak of the narrow line is at the expected wavenumber position for films #1 and #2, but for films #3 and #4 the narrow line is downshifted to 1320 cm^{-1}. The full width at half maximum (FWHM) of the narrow line is $\leq$12 cm^{-1} for all films.

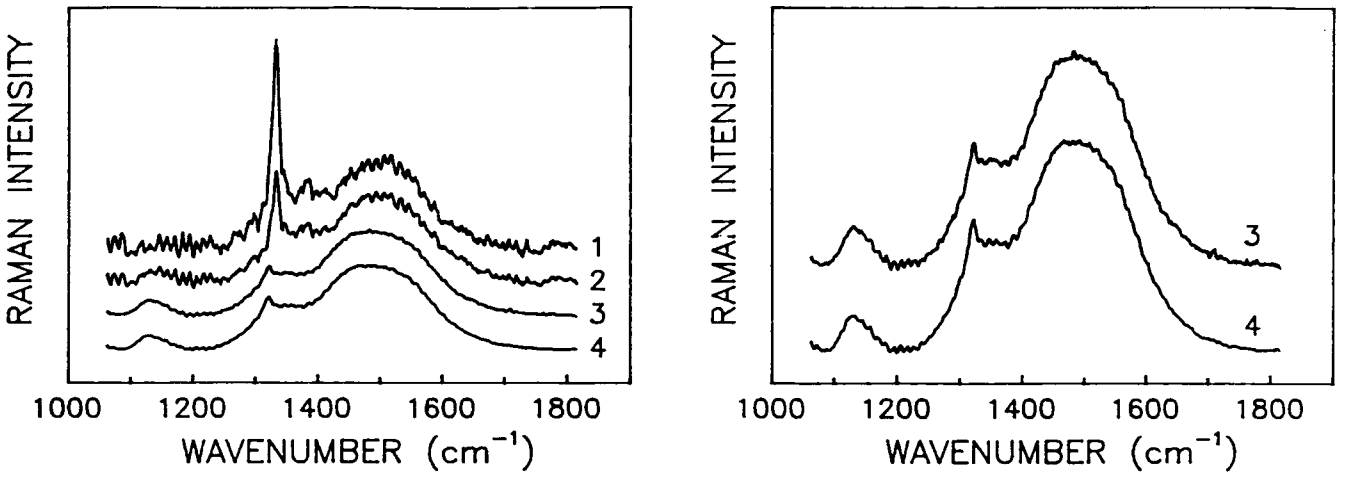

Fig. 2. Raman spectra of diamond windows, excited by 514.5 nm (2.410 eV) line of Ar^+ laser with incident intensity of ~0.1 W. Photoluminescence backgrounds have been subtracted; spectra are offset vertically and rescaled for ease of comparison. (a) Windows #1 to #4. (b) Windows #3 and #4; expanded scale.

The broad peak at ~1500 cm^{-1}, with a FWHM of 200 cm^{-1}, occurs in all four films. The peak position of the broad peak appears to be slightly lower for films #3 and #4 than for films #1 and #2. The spectra of films #3 and #4 also contain another distinct peak on the low-wavenumber side of the diamond line. The low-wavenumber peak is located at 1130 cm^{-1} and has a FWHM of ~50 cm^{-1}. This peak may also occur in the spectrum of film #2, but is difficult to discern in the latter spectrum because of the poorer signal-to-noise ratio. The origin of the 1130 cm^{-1} and 1500 cm^{-1} peaks will be discussed later.

4. DATA ANALYSIS

4.1. Transmittance and reflectance of a thin film with rough surfaces

In order to obtain the optical constants of these films from an analysis of the specular transmittance (T) and reflectance (R_1 and R_2) spectra shown in Fig. 1, one must first write down the equations that express T, R_1, and R_2 as functions of the optical constants (n, k) or (n, α) and of surface scatter losses. These equations can be derived from the well-known equations for the transmittance and reflectance of a thin film without surface scatter, and reduce to the scatter-free equations when the loss factors S_T, S_{EX}, and S_{IN} (defined below) are equal to unity. It is assumed here that the angle of incidence is normal to the film surface, and that there are air interfaces on both sides of the film. The derivation of these equations will be discussed in more detail in a future publication.[8]

$$T = A\tau \,/\, [1 - 2B\tau \cos(\Phi+2\delta) + B^2\tau^2] \qquad (1)$$

$$R_1 = [C_1^2 - 2C_1D_1\tau \cos(\Phi) + D_1^2\tau^2] \,/\, [1 - 2B\tau \cos(\Phi+2\delta) + B^2\tau^2] \qquad (2)$$

$$R_2 = [C_2^2 - 2C_2D_2\tau \cos(\Phi) + D_2^2\tau^2] \,/\, [1 - 2B\tau \cos(\Phi+2\delta) + B^2\tau^2] \qquad (3)$$

The parameters of Eqs. (1)-(3) are defined as follows:

$$A = S_{T1}^2 \, S_{T2}^2 \, T_0 \quad (4) \qquad B = S_{IN1} \, S_{IN2} \, R_0 \quad (5)$$

$$C_1 = S_{EX1} \sqrt{R_0} \quad (6) \qquad D_1 = [(1-R_0)S_{T1}+R_0 S_{EX1} S_{IN1}] \, S_{IN2} \sqrt{R_0} \quad (7)$$

$$C_2 = S_{EX2} \sqrt{R_0} \quad (8) \qquad D_2 = [(1-R_0)S_{T2}+R_0 S_{EX2} S_{IN2}] \, S_{IN1} \sqrt{R_0} \quad (9)$$

$$\tau = e^{-\alpha d} = e^{-4\pi k d/\lambda} \quad (10) \qquad \Phi = 4\pi n d/\lambda \quad (11)$$

$$\delta = \tan^{-1}[2k/(n^2+k^2-1)] \quad (\text{in range } -\pi/2 \le \delta \le \pi/2) \quad (12)$$

$$T_0 = 16(n^2+k^2) \, / \, [(n+1)^2+k^2]^2 \quad (13) \qquad R_0 = [(n-1)^2+k^2] \, / \, [(n+1)^2+k^2] \quad (14)$$

$$S_{EXi} = \exp\{-\tfrac{1}{2}(4\pi\sigma_i/\lambda)^2\} \quad (15) \qquad S_{INi} = \exp\{-\tfrac{1}{2}(4\pi n\sigma_i/\lambda)^2\} \quad (16)$$

$$S_{Ti} = \exp\{-\tfrac{1}{2}[2\pi(n-1)\sigma_i/\lambda]^2\} \quad (\text{for } i = 1,2) \quad (17)$$

In these equations, d is the film thickness; λ is the free-space wavelength; and σ_1 and σ_2 are, respectively, the root-mean-squared (r.m.s.) surface roughnesses of the top and bottom surfaces. Some of the defined quantities can be interpreted as follows: τ is the internal transmittance due to bulk absorption losses; Φ (or $\Phi + 2\delta$) determines the periodicity of the interference fringe pattern; T_0 is the scatter-free and absorption-free film transmittance, which is less than unity because of surface reflection losses; R_0 is the scatter-free surface reflectivity; and S_{EXi}, S_{INi}, and S_{Ti} are the surface-scatter loss factors for, respectively, external reflectance (with incident and reflected beams outside the film), internal reflectance (with incident and reflected beams inside the film), and transmittance (in either direction). In the above equations, notice that if $k \ll n$, then the parameters T_0, R_0, A, B, C_1, D_1, C_2, D_2 are effectively independent of k, and $\delta \approx 0$.

According to Eqs. (15)-(17), the surface-scatter losses at a given wavelength depend only on the refractive index and the surface roughnesses σ_1 and σ_2. Our model for the surface-scatter losses [Eqs. (15)-(17)] is taken from the previous work of Filinski[9] and Gatesman et al.[10] A similar, but more empirical, model for the effects of surface scatter on optical properties was presented by Bi et al.[11]

As stated in the Experimental Results section, the angle of incidence (θ) is 11° to the normal for reflectance measurements. The parameters Φ, τ, and S_{EX}, S_{IN}, and S_T should thus be modified in Eqs. (2) and (3) to account for the θ-dependence of the optical path lengths. (The factors T_0 and R_0 are also dependent on θ, and, for $\theta > 0$, on polarization, but these dependencies have little effect on T and R for small angles, and will thus be neglected.) The θ-dependent parameter values are

$$\Phi = 4\pi n_\theta d/\lambda \quad (18) \qquad \tau = \exp\{-\alpha d(n/n_\theta)\} \quad (19)$$

$$S_{EXi} = \exp\{-\tfrac{1}{2}(4\pi\sigma_i \cos(\theta)/\lambda)^2\} \quad (20) \qquad S_{INi} = \exp\{-\tfrac{1}{2}(4\pi n_\theta \sigma_i/\lambda)^2\} \quad (21)$$

$$S_{Ti} = \exp\{-\tfrac{1}{2}[2\pi(n_\theta - \cos(\theta))\sigma_i/\lambda]^2\} \quad (22) \qquad \text{where } n_\theta = (n^2 - \sin^2(\theta))^{1/2} \quad (23)$$

4.2. Determination of optical constants

In order to fit Eqs. (1)-(3) to the experimental data, it is necessary to express n(E) and α(E) as specific functions with adjustable parameters. The function used

Robins

to represent n(E) is

$$n(E) = n_0 + \Delta n(E) = n_0 + n_1 E^2 + n_2 E^4/[1-n_3 E^2] \quad (24)$$

The parameter values for single-crystal diamond, obtained by fitting standard refractive index data (tabulated in a handbook[12]), are n_0=2.377, n_1=0.0086 $(eV)^{-2}$, n_2=4.7x10^{-5} $(eV)^{-4}$, and n_3=0.0155 $(eV)^{-2}$. The function used to represent $\alpha(E)$ is

$$\alpha(E) = \alpha_{a\text{-}C} + \alpha_{bandgap} \quad (25)$$

$$\text{where} \quad \alpha_{a\text{-}C}(E) = \alpha_{01}(E - E_{01})^2/E \quad (\text{for } E \geq E_{01}) \quad (26)$$

$$\text{and} \quad \alpha_{bandgap}(E) = \alpha_{02}\exp(E/E_{02}) + c_3\alpha_{dia}(E) \quad (27)$$

The adjustable parameters of $\alpha(E)$ are α_{01}, E_{01}, α_{02}, E_{02}, and c_3. The functional form of Eq. (26), the Taucs function, is often used to fit the absorption spectra of amorphous semiconductors or insulators. In Eq. (27), $\alpha_{dia}(E)$ is the above-bandgap absorption spectrum of type IIa single-crystal diamond.[12]

In principle, all free parameters may be determined by a simultaneous fit of the full T, R_1, and R_2 spectra to Eqs. (1)-(3). This procedure worked well for $\alpha(E)$, σ_1 and σ_2, but not for n(E) and d. The latter quantities were, instead, determined by selective fitting to portions of the experimental spectra. First, n_0 was found by fitting the low-energy ($E \leq 2$ eV) portion of the transmittance spectrum. The dispersive part of n(E), scatter and absorption all become small at low photon energy. The following equation thus holds in the low photon energy limit:

$$T_{min} / T_{max} = 4n_0^2 / (n_0^2+1)^2 \quad (28)$$

where T_{min} is the transmittance at an interference minimum and T_{max} is the transmittance at an interference maximum. The parameters n_1 and n_2 and the film thickness d were then determined from the photon energy dependence of the interference fringe frequency. (Variation of n_3 did not improve the fit to the data; n_3 was therefore fixed at its single-crystal value.)

$$\Phi(E) = 4\pi n(E)d/\lambda = 4\pi n_0 d/\lambda + 4\pi d/\lambda\{n_1 E^2 + n_2 E^4/[1-n_3 E^2]\} \quad (29)$$

The interference fringe amplitude at high photon energy is larger for R_1 than for R_2 or T; therefore, only R_1 data were used to find n_1 and n_2.

Table I lists the fitted values of all parameters. The difference between the fitted values of n(E) [Eq. (24)] for windows #1 to #3 and for single-crystal diamond is plotted in Fig. 3. It can be seen that the refractive indices of the films are similar to that of single-crystal diamond. The difference is largest (n is reduced most) for film #3. We could not make an accurate estimate of $\Delta n(E)$ for window #4 because of the small amplitude of the interference fringes at high photon energy [see Fig. 1(d)]. Therefore, the results shown in Fig. 3 do not include window #4. Because of other similarities, however, it is likely that $\Delta n(E)$ of window #4 closely resembles that of window #3.

After n(E) and d have been obtained, $\alpha(E)$, σ_1 and σ_2 are found by a simultaneous least-squares fit of Eqs. (1)-(3), and Eqs. (25)-(27) for $\alpha(E)$, to the experimental data. (The fitted data points were spaced every 0.01 eV from 0.5 to 6.5 eV.) The films are found to be weakly absorbing in the sense that $k \ll n$ (where $k = \alpha\lambda/4\pi$). In

Robins

Table I. Film thicknesses, r.m.s. surface roughnesses, and optical constant parameters for CVD diamond windows (parameters that determine n(E) and $\alpha(E)$ are defined in the text). Symbol (X) indicates undetermined parameters; (-) indicates undefined parameters for single crystal.

Parameter	film #1	film #2	film #3	film #4	single crystal
d (μm)	0.66	0.46	0.42	1.90	-
σ_1 (μm) (top)	0.0332	0.0218	0.0138	0.0179	-
σ_2 (μm) (bottom)	0.0078	0.0067	0.0049	0.0062	-
n_0	2.374	2.364	2.334	2.30	2.377
n_1	9.4×10^{-3}	8.3×10^{-3}	7.1×10^{-3}	X	8.6×10^{-3}
n_2	4.7×10^{-5}	4.7×10^{-5}	4.4×10^{-5}	X	4.7×10^{-5}
α_{01} (cm^{-1} eV^{-1})	X	2190	6340	7620	0.0
E_{01} (eV)	X	2.08	1.14	1.07	-
α_{02} (cm^{-1})	X	2.0×10^{-4}	0.41	X	0.0
E_{02} (eV)	X	0.347	0.564	X	-
c_3	X	0.54	0.0	X	1.0

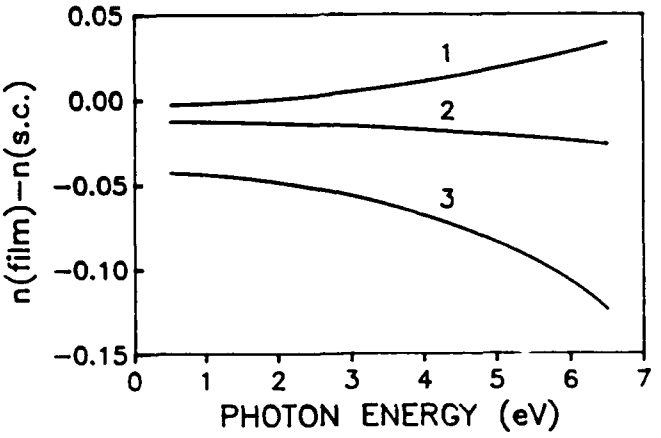

Fig. 3. Differences between fitted refractive indices of windows #1 to #3 and of single crystal, $n(E)-n_{sc}(E)$. These curves were obtained by fitting data (or, for single crystal, handbook values[12] of n) to the form given by Eq. (24).

Robins 8

the weakly absorbing case, the fitted values of $\alpha(E)$ can be refined by the following calculation. First, rewrite Eq. (1) for the fitted transmittance:

$$T_{fit}(E) = A\tau_{fit}(E) \,/\, [1 - 2B\tau_{fit}(E)\cos(\Phi+2\delta) + B^2\tau_{fit}^2(E)] \tag{30}$$

As pointed out earlier, the parameters A, B, and $(\Phi+2\delta)$ are virtually independent of k (or α) when $k \ll n$; only the internal transmittance τ is dependent on α. We can therefore define new functions $(\alpha'(E), \tau'(E))$ that precisely match the experimental transmittance $T_{exp}(E)$ while leaving A, B, and $(\Phi+2\delta)$ unchanged.

$$T_{exp}(E) = A\tau'(E) \,/\, [1 - 2B\tau'(E)\cos(\Phi+2\delta) + B^2\tau'^2(E)] \tag{31}$$

$$\text{where} \qquad \tau'(E) = \exp\{-\alpha'(E)d\} = \exp\{-(\alpha_{fit}(E) + \Delta\alpha(E))d\} \tag{32}$$

Eqs. (30), (31), and (32) can be solved for $\alpha'(E)$:

$$\alpha'(E) = \alpha_{fit}(E) + (1/d)\log\{\tfrac{1}{2}[x + y + 1 + ((x+1)^2+2y(x-1)+y^2)^{1/2}]\} \tag{33}$$

$$\text{where} \quad x = A\tau_{fit}(E)\,[1/T_{exp}(E) - 1/T_{fit}(E)] \quad \text{and} \quad y = [B\,\tau_{fit}(E)]^2 \tag{34}$$

Improved estimates for the adjustable parameters of Eqs. (25)-(27) can be obtained by refitting these equations to the refined absorption spectra $\alpha'(E)$. These improved estimates are the ones listed in Table I. The absorption spectra $\alpha'(E)$ of films #2, #3, and #4, as obtained from Eqs. (30)-(34), are plotted in Fig. 4. (It was not possible to determine $\alpha(E)$ for film #1 because of the large amount of surface scatter in that film.) The intrinsic absorption spectrum of single-crystal diamond (obtained from type IIa natural diamond gems) is also shown in Fig. 4.

According to the results shown in Fig. 4, the absorption coefficient is a monotonically increasing function of photon energy. Two components are discernable in the absorption spectra of films #2 and #3, a broad low-energy absorption that increases almost linearly with increasing photon energy, and a relatively steep increase in the vicinity of 5.5 eV. These two components correspond respectively to the two terms $\alpha_{a\text{-}C}$ and $\alpha_{bandgap}$ in Eq. (25). Films #3 and #4 were grown under identical conditions, except that film #4 was grown for a longer time. The latter two films are thus expected to have similar absorption coefficients. The experimental results in the region below 5.5 eV meet this expectation; the absorption coefficient of film #4 cannot be determined in the region above 5.5 eV because of its greater thickness and correspondingly lower transmittance.

The calculated values of the bandgap component of the absorption spectra of films #2 and #3 are plotted in Fig. 5, together with the absorption spectrum of single-crystal diamond. The latter spectrum is the same one shown in Fig. 4; the former spectra are calculated from the equation

$$\alpha'_{bandgap}(E) = \alpha'(E) - \alpha_{a\text{-}C}(E) \tag{35}$$

Notice that in a narrow spectral region just above 5.5 eV, the magnitude of $\alpha'_{bandgap}$ for film #2 is very similar to the magnitude of α for single-crystal diamond. However, $\alpha'_{bandgap}$ increases more rapidly with increasing photon energy in film #2 than in single-crystal diamond; $\alpha'_{bandgap}$ of film #2 thus diverges significantly from single-crystal values in the 6-6.5 eV region.

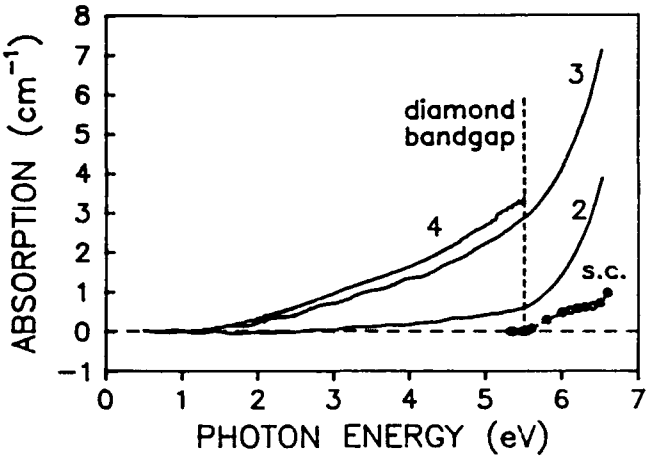

Fig. 4. Absorption spectra $\alpha'(E)$ of diamond windows #2 to #4, calculated by method described in text. Spectrum of type IIa single crystal is plotted for comparison.

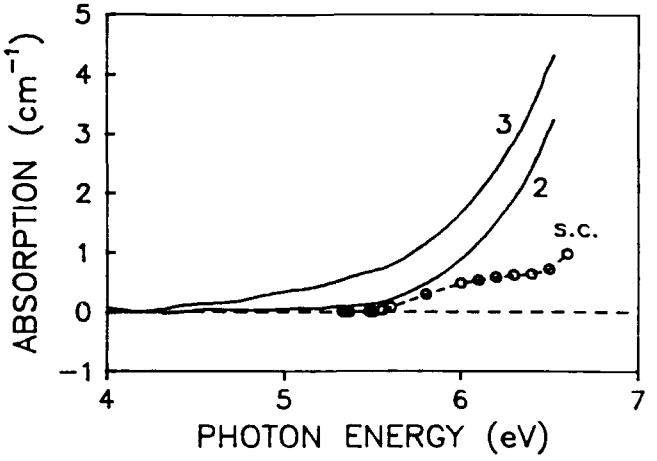

Fig. 5. Bandgap absorption spectra of diamond windows #3 and #4, obtained by subtracting the low-energy absorption, $\alpha_{a\text{-}C}(E)$, from the total absorption $\alpha'(E)$. Spectrum of type IIa single crystal is shown for comparison.

5. DISCUSSION

The refractive indices of the most defective films lie within 4% of the refractive index of single-crystal diamond. The refractive index is thus relatively insensitive to the defect structures or nondiamond phases that are present in these specimens. On the other hand, the defective nature of these films has two very significant effects on the optical absorption spectrum. First, there is the presence of the broad absorption at low photon energy (the component labelled $\alpha_{a\text{-}C}$). Second, there is the steeper-than-expected increase in absorption near 5.5 eV.

The Taucs function [Eq. (26)] is widely accepted as a good approximation for the absorption spectra of "diamondlike" amorphous carbon and amorphous hydrogenated carbon materials with mixed sp^2 and sp^3 bonding, as well as other noncrystalline semiconductors such as amorphous silicon. The presence of this absorption thus suggests the presence in our films of an amorphous carbon phase similar to "diamondlike" carbon; that is why we chose the symbol $\alpha_{a\text{-}C}$. The parameter E_{01}, the Taucs energy gap, is believed to be anticorrelated with the extent of the largest clusters of sp^2-bonded carbon atoms.[13] The shorter is the maximum cluster length, the larger is the value of E_{01}. The fitted value of 2.08 eV for film #2 is consistent with a maximum cluster length of three aromatic rings; the value of 1.1 eV for films #3 and #4 is consistent with a maximum length of six rings.

The absorption coefficient increases more rapidly with increasing photon energy above 5.5 eV (the indirect bandgap of diamond) in films #2 and #3 than in single-crystal diamond, and the rate of increase is approximately exponential (see Eq. (27), Fig. 5, and Table 1). A possible explanation for the excess above-bandgap absorption lies in the existence of disorder-induced band tails of localized states above the valence band edge and/or below the conduction band edge. Transitions involving such band tail states may give rise to extra absorption below the direct gap at 7.2 eV. The density of states in the band tails typically falls

exponentially away from the band edges; the exponential form of the above-bandgap absorption thus tends to support the band tail model. The width of the exponential, E_{02}, is larger in film #3 than in film #2, suggesting that the band tails are broader in the former film. In a previous study of the optical properties of polycrystalline diamond films, Bi et al.[11] also observed an exponential rise in optical absorption in the neighborhood of 5.5 eV.

The optical absorption data suggest that at least two phases are present: first, a highly defective crystalline diamond phase with predominantly sp^3 bonding; and, second, an amorphous carbon phase with mixed sp^2 and sp^3 bonding. This is consistent with the results of the Raman spectra, where the narrow 1332 cm^{-1} line is due to crystalline diamond; the broad 1500 cm^{-1} band is due to sp^2-bonded carbon in an amorphous phase; and the 1130 cm^{-1} band and the large downshift of the (nominal) 1332 cm^{-1} line is believed to be due to a partial breakdown of crystalline order in the diamond phase ("nanocrystalline diamond"). If two phases are present, then they must be segregated on some length scale, which is not yet known.

The results of this study may have some practical significance for IR optical applications of CVD diamond. The most defective films, films #3 and #4, are the most strongly absorbing in the visible and near-IR, but also have the smoothest surfaces and thus suffer least from optical scatter (see Table 1 and Fig. 4). At least for film thicknesses ≤ 2 μm, these films absorb very little below 1.1 eV, the Taucs energy gap [Eq. (26)]. Films with these properties should make good anti-reflection coatings for silicon optics because of their freedom from both optical absorption and optical scatter at photon energies below the bandgap of silicon (which, fortuitously, is also 1.1 eV).

6. CONCLUSIONS

The optical constants of fine-grained polycrystalline diamond windows grown by microwave-plasma-assisted CVD were determined by analysis of transmittance, top-surface reflectance, and bottom-surface reflectance spectra in the 0.5-6.5 eV photon energy range. By fitting the data to a model that takes surface scatter into account, estimates of the r.m.s. surface roughnesses of the top and bottom surfaces were also obtained. The refractive indices were found to be comparable to or slightly less than the refractive index of single-crystal diamond. The absorption spectra were found to consist of two components: a low-energy component, similar to that of "diamondlike" amorphous carbon materials, described by the Taucs function $\alpha(E) = \alpha_{01}(E-E_{01})^2/E$ (for $E>E_{01}$); and a high-energy component that increases sharply above the indirect bandgap of diamond (5.5 eV). The high-energy component increases at an approximately exponential rate with increasing photon energy, unlike the bandgap absorption of single-crystal diamond; this behavior is attributed to disorder-induced band tail states. These results suggest that the films contain both a highly defective crystalline diamond phase and a "diamondlike" amorphous carbon phase; the length scale for phase inhomogeneity is not known.

7. ACKNOWLEDGEMENTS

This work was supported in part by the Office of Naval Research.

8. REFERENCES

1. A. Feldman and L. H. Robins, "Critical Assessment of Optical Properties of CVD Diamond Films", Proc. of the 1st Int. Conf. on the Applications of Diamond Films and Related Mater., Auburn, AL, 1991 (in press)

2. T. Feng, "Co relation of Optical Properties and Surface Roughness of Polycrystalline Diamond Films", in Diamond Optics II, ed. by A. Feldman and S. Holly, Proc. SPIE 1146, 159 (1989)

3. H. Windischmann and G. F. Epps, "Properties of Diamond Membranes for X-Ray Lithography", J. Appl. Phys. 68, 5665 (1990)

4. A. B. Harker, J. Flintoff and J. F. DeNatale, "The Polishing of Polycrystalline Diamond Films", in Diamond Optics III, ed. by A. Feldman and S. Holly, Proc. SPIE 135, 222 (1990)

5. T. P. Thorpe, A. A. Morrish, L. M. Hanssen, J. E. Butler and K. A. Snail, "Growth, Polishing and Optical Scatter of Diamond Thin Films", in Diamond Optics III, ed. by A. Feldman and S. Holly, Proc. SPIE 135, 230 (1990)

6. The abrasive polishing technique was initially described to us by D. J. Pickrell of Penn State University (private communication)

7. L. H. Robins, E. N. Farabaugh and A. Feldman, "Lineshape Analysis of the Raman Spectrum of Diamond Films Grown by Hot-Filament and Microwave-Plasma Chemical Vapor Deposition", J. Mater. Res. 5, 2456 (1990)

8. Robins, L. H., Feldman, A., and Farabaugh, E. N., to be published

9. I. Filinski, "The Effects of Sample Imperfections on Optical Spectra", Phys. Stat. Sol. B49, 577 (1972)

10. A. J. Gatesman, R. H. Giles, J. Waldman, L. P. Bourget and R. Post, "Optical Properties of Polycrystalline Diamond Films in the Far-Infrared", Diamond Optics III, ed. by A. Feldman and S. Holly, Proc. SPIE 1325, 170 (1990)

11. X. X. Bi, P. C. Eklund, J. G. Zhang, A. M. Rao, T. A. Perry and C. P. Beetz, "Optical Properties of Chemical-Vapor-Deposited Diamond Films", J. Mater. Res. 5, 811 (1990)

12. D. F. Edwards and H. R. Philipp, "Cubic Carbon (Diamond)", in Handbook of Optical Constants of Solids, ed. by E. D. Palik (Academic Press, 1985), p. 665

13. J. Robertson, "Amorphous Carbon", Adv. Phys. 35, 317 (1986)

6 March 1991

FY91 ONR DOMES ARI CONTRACTORS

Dr. Duncan W. Brown
Advanced Technology Materials, Inc.
520-B Danbury Road
New Milford, CT 06776
(203) 355-2681

Dr. Mark A. Cappelli
Stanford University
Mechanical Engineering Dept.
Stanford, CA 94305
(415) 723-1745

Dr. R. P. H. Chang
Materials Science & Engineering Dept.
2145 Sheridan Road
Evanston, IL 60208
(312) 491-3598

Dr. Bruce Dunn
UCLA
Chemistry Department
Los Angeles, CA 90024
(213) 825-1519

Dr. Al Feldman
Leader, Optical Materials Group
Ceramics Division
Materials Science & Engineering Lab
NIST
Gaithersburg, MD 20899
(301) 975-5740

Dr. John Field
Department of Physics
University of Cambridge
Cavendish Laboratory
Madingley Road
Cambridge CB3 OHE
England
44-223-337733, ext. 7318

Dr. William A. Goddard, III
Director, Materials and Molecular
Simulation Center
Beckman Institute
California Institute of Technology
Pasadena, CA 91125
(818) 356-6544
Fax: (818) 568-8824

Dr. David Goodwin
California Institute of Technology
Mechanical Engineering Dept.
Pasadena, CA 91125
(818) 356-4249

Dr. Alan Harker
Rockwell Int'l Science Center
1049 Camino Dos Rios
P.O. Box 1085
Thousand Oaks, CA 91360
(805) 373-4131

Mr. Stephen J. Harris
General Motors Research Laboratories
Physical Chemistry Department
30500 Mound Road
Warren, MI 48090-9055
(313) 986-1305
Fax: (313) 986-8697
E-mail: sharris@gmr.com

Dr. Rudolph A. Heinecke
Standard Telecommunication
Laboratories, Ltd.
London Road
Harlow, Essex CM17 9MA
England
44-279-29531, ext. 2284

Dr. Kelvin Higa
Code 3854
Naval Weapons Center
China Lake, CA 93555-6001

Enclosure (1)

Dr. Curt E. Johnson
Code 3854
Naval Weapons Center
China Lake, CA 93555-6001
(619) 939-1631

Dr. J. J. Mecholsky, Jr.
University of Florida
Materials Science & Engineering Dept.
256 Rhines Hall
Gainesville, FL 32611
(904) 392-1454

Dr. Rishi Raj
Cornell University
Materials Science & Engineering Dept.
Ithaca, NY 14853
(607) 255-4040

Dr. Rustum Roy
Pennsylvania State University
Materials Research Laboratory
University Park, PA 16802
(814) 865-2262

Dr. James A. Savage
Royal Signals & Radar Establishment
St. Andrews Road
Great Malvern, Worcs WR14.3PS
England
01-44-684-895043

Dr. Y. T. Tzeng
Auburn University
Electrical Engineering Dept.
Auburn, AL 36849
(205) 884-1869

Dr. Terrell A. Vanderah
Code 3854
Naval Weapons Center
China Lake, CA 93555-6001
(619) 939-1654

Dr. George Walrafen
Howard University
Chemistry Department
525 College Street N.W.
Washington, D.C. 20059
(202) 636-6897/6564

Dr. Aaron Wold
Brown University
Chemistry Department
Providence, RI 02912
(401) 863-2857

Dr. Wally Yarborough
Pennsylvania State University
Materials Research Laboratory
University Park, PA 16802
(814) 865-7102

6 March 1991

DISTRIBUTION LIST

Mr. James Arendt
Hughes Aircraft Company
8433 Fallbrook Ave. 270/072
Canoga Park, CA 91304
(838) 702-2890

Mr. Larry Blow
General Dynamics
1525 Wilson Blvd., Suite 1200
Arlington, VA 22209
(703) 284-9107

Mr. Ellis Boudreaux
Code AGA
Air Force Armament Laboratory
Eglin AFB, FL 32542

Dr. Duncan W. Brown
Advanced Technology Materials, Inc.
520-B Danbury Road
New Milford, CT 06776
(203) 355-2681

Dr. Mark A. Cappelli
Stanford University
Mechanical Engineering Dept.
Standford, CA 94305
(415) 723-1745

Dr. R. P. H. Chang
Materials Science & Engineering Dept.
2145 Sheridan Road
Evanston, IL 60208
(312) 491-3598

Defense Documentation Center
Cameron Station
Alexandria, VA 22314
(12 copies)

Dr. Al Feldman
Leader, Optical Materials Group
Ceramics Division
Materials Science & Engineering Lab
NIST
Gaithersburg, MD 20899
(301) 975-5740

Dr. John Field
Department of Physics
University of Cambridge
Cavendish Laboratory
Madingley Road
Cambridge CB3 OHE
England
44-223-337733, ext. 7318

Dr. William A. Goddard, III
Director, Materials and Molecular
Simulation Center
Beckman Institute
California Institute of Technology
Pasadena, CA 91125
(818) 356-6544
Fax: (818) 568-8824

Dr. David Goodwin
California Institute of Technology
Mechanical Engineering Dept.
Pasadena, CA 91125
(818) 356-4249

Dr. Kevin Gray
Norton Company
Goddard Road
Northboro, MA 01532
(508) 393-5968

Mr. Gordon Griffith
WRDC/MLPL
Wright-Patterson AFB, OH 45433

Dr. H. Guard
Office of Chief of Naval Research
(ONR Code 1113PO)
800 North Quincy Street
Arlington, VA 22217-5000

Dr. Alan Harker
Rockwell Int'l Science Center
1049 Camino Dos Rios
P.O. Box 1085
Thousand Oaks, CA 91360
(805) 373-4131

Mr. Stephen J. Harris
General Motors Research Laboratories
Physical Chemistry Department
30500 Mound Road
Warren, MI 48090-9055
(313) 986-1305
Fax: (313) 986-8697
E-mail: sharris@gmr.com

Dr. Rudolph A. Heinecke
Standard Telecommunication
Laboratories, Ltd.
London Road
Harlow, Essex CM17 9MA
England
44-279-29531, ext. 2284

Dr. Curt E. Johnson
Code 3854
Naval Weapons Center
China Lake, CA 93555-6001
(619) 939-1631

Dr. Larry Kabacoff (Code R32)
Officer in Charge
Naval Surface Weapons Center
White Oak Laboratory
10901 New Hampshire
Silver Spring, MD 20903-5000

Mr. M. Kinna
Office of Chief of Naval Research
(ONT Code 225)
800 North Quincy Street
Arlington, VA 22217-5000

Dr. Paul Klocek
Texas Instruments
Manager, Advanced Optical Materials Branch
13531 North Central Expressway
P.O. Box 655012, MS 72
Dallas, Texas 75268
(214) 995-6865

Ms. Carol R. Lewis
Jet Propulsion Laboratory
4800 Oak Grove Drive
Mail Stop 303-308
Pasadena, CA 91109
(818) 354-3767

Dr. J. J. Mecholsky, Jr.
University of Florida
Materials Science & Engineering Dept.
256 Rhines Hall
Gainesville, FL 32611
(904) 392-1454

Dr. Russ Messier
Pennsylvania State University
Materials Research Laboratory
University Park, PA 16802
(814) 865-2262

Mr. Mark Moran
Code 3817
Naval Weapons Center
China Lake, CA 93555-6001

Mr. Ignacio Perez
Code 6063
Naval Air Development Center
Warminster, PA 18974
(215) 441-1681

Mr. C. Dale Perry
U.S. Army Missile Command
AMSMI-RD-ST-CM
Redstone Arsenal, AL 35898-5247

Mr. Bill Phillips
Crystallume
125 Constitution Drive
Menlo Park, CA 94025
(415) 324-9681

Dr. Rishi Raj
Cornell University
Materials Science & Engineering Dept.
Ithaca, NY 14853
(607) 255-4040

Dr. M. Ross
Office of Chief of Naval Research
(ONR Code 1113)
800 North Quincy Street
Arlington, VA 22217-5000

Dr. Rustum Roy
Pennsylvania State University
Materials Research Laboratory
University Park, PA 16802
(814) 865-2262

Dr. James A. Savage
Royal Signals & Radar Establishment
St. Andrews Road
Great Malvern, Worcs WR14.3PS
England
01-44-684-895043

Mr. David Siegel
Office of Chief of Naval Research
(ONT Code 213)
800 North Quincy Street
Arlington, VA 22217-5000

Dr. Keith Snail
Code 6520
Naval Research Laboratory
Washington, D.C. 20375
(202) 767-0390

Dr. Y. T. Tzeng
Auburn University
Electrical Engineering Dept.
Auburn, AL 36849
(205) 884-1869

Dr. George Walrafen
Howard University
Chemistry Department
525 College Street N.W.
Washington, D.C. 20054
(202) 806-6897/6564

Mr. Roger W. Whatmore
Plessey Research Caswell Ltd.
Towcester Northampton NN128EQ
England
(0327) 54760

Dr. Charles Willingham
Raytheon Company
Research Division
131 Spring Street
Lexington, MA 02173
(617) 860-3061

Dr. Robert E. Witkowski
Westinghouse Electric Corporation
1310 Beulah Road
Pittsburgh, PA 15235
(412) 256-1173

Dr. Aaron Wold
Brown University
Chemistry Department
Providence, RI 02912
(401) 863-2857

Mr. M. Yoder
Office of Chief of Naval Research
(ONR Code 1114SS)
800 North Quincy Street
Arlington, VA 22217-5000